ISBN: 978-3-95450-247-9 ISSN: 2673-5490 doi: 10.18429/JACoW-IPAC2024-WEPR57

SIMULATIONS OF INCOHERENT EFFECTS DRIVEN BY ELECTRON CLOUDS FORMING IN THE INNER TRIPLETS OF THE LARGE HADRON COLLIDER

K. Paraschou*, G. Iadarola, L. Mether, CERN, Geneva, Switzerland

Abstract

During Run 2 and Run 3 of the Large Hadron Collider (LHC), slow losses from electron cloud (e-cloud) effects have been systematically observed during the full duration of fills with closely-spaced proton bunches. In particular, these effects had been found to depend strongly on the crossing angle of the two beams and the value of the betatron functions in the interaction points. Due to this observation, the main cause of this effect was attributed to the non-linear forces induced by electron clouds forming in the vacuum chamber of the LHC Inner Triplet quadrupole magnets. In this contribution, electron cloud buildup simulations reveal that the induced forces depend strongly on the transverse coordinates of the beam particles, on time, as well as on the longitudinal coordinate within the Inner Triplet. Finally, non-linear maps are generated based on the buildup simulations, and the effect of these forces on the motion of the protons is simulated.

INTRODUCTION

The bunch-by-bunch pattern of incoherent slow beam losses during physics operation (Run 2) at the LHC was analysed in Refs. [1–3]. The analysis revealed that a significant fraction of them are attributed to electron clouds (e-clouds) [4] forming in the Inner Triplet (IT) quadrupole magnets (final focusing quadrupoles) around Interaction Points (IPs) 1 and 5. The observations leading to this conclusion were the dependence of the losses on:

1. the position of the bunch in the bunch train (with losses growing from the head to the tail),
2. the presence of both beams in the chamber of the IT,
3. the crossing scheme which prevents head-on collisions of the beams away from the interaction point,
4. the large betatron functions in the ITs, necessary to achieve small beam size in the IPs.

Exactly the same reasons complicate the simulation of the electron cloud effects in the IT. At any longitudinal position inside the IT, the two counter-rotating beams will be arriving at different times, at different transverse positions defined by the crossing scheme and with different beam sizes due to the changing betatron functions. This necessitates the splitting of the IT in numerous longitudinal slices and the simulation of the e-cloud formation in each of the slices [5]. All these influence the formation of the e-cloud. Figure 1 illustrates the number of electrons from electron cloud buildup simulations along the different longitudinal positions in the IT right of IP 1. In addition to the above reasons, a clear distinction appears also between regions with a quadrupolar magnetic field (shaded regions) and drift spaces. Finally, it can be noticed that the e-cloud buildup is suppressed in locations with long-range encounters between the two beams (dashed vertical lines).

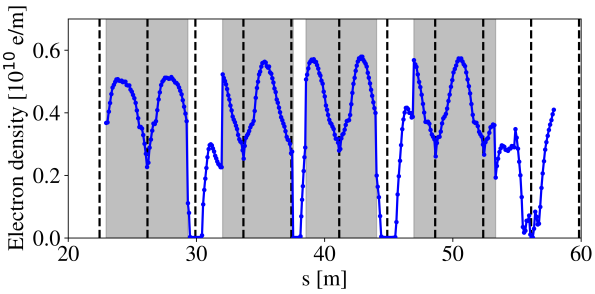

Figure 1: Electron density versus the longitudinal position in the IT right of IP 1.

To simulate the incoherent effect of this e-cloud, we follow the same strategy that was followed for the simulation of incoherent e-cloud effects for the LHC in its injection energy configuration in Refs. [4, 6–8]. The simulations were performed using the Xsuite software [9] with Graphics Processing Units (GPU), applying a weak-strong approximation where the e-cloud evolves during the passage of the bunch, but this evolution remains identical for the full simulation time. This is justified by the fact that incoherent effects are very slow, and the beam profiles do not change noticeably during the simulation period. The interaction between protons and e-cloud was simulated by importing the time-dependent scalar potential on a grid, as produced by the e-cloud buildup Particle-in-Cell simulations performed with the PyECLOUD software [10]. To ensure the symplecticity of the interaction, a tricubic interpolation scheme was used on the discrete points consisting the scalar potential. Moreover, the non-linear lattice model of the LHC was used in the simulations in Refs. [4, 6–8] where, for example, the interaction with the e-cloud forming in an arc quadrupole was simulated at the location of each arc quadrupole. A detailed description of these simulations is available in Ref. [7].

Unfortunately, the e-cloud formation varies significantly among the slices of the IT and a large number of slices is necessary to resolve the structure of the e-cloud in the IT. This prevents a direct "brute force" simulation as the memory consumption can easily exceed several terabytes. In this work, we define a method by employing basic properties of Lie transformations [11] to combine the different slices of each IT into a single effective scalar potential that can be used to describe the e-cloud in the entire IT. A similar method was used in the past to study long-range beam-beam effects in the LHC [12].

* konstantinos.paraschou@cern.ch

ISBN: 978-3-95450-247-9 ISSN: 2673-5490 doi: 10.18429/JACoW-IPAC2024-WEPR57

EFFECTIVE E-CLOUD IN THE IT

A Lie transformation is defined by the exponential of the Poisson bracket operator $(: f :)$, of a generating function f [11]. In the e-cloud case, the scalar potential ϕ is the generating function [13]. Let f_{ij} be the function that generates the transformation that transports a particle from a location labelled i to a location labelled j. The transformation from location i to k, with an e-cloud interaction at an intermediate location j is written as:

$$e^{:f_{ij}:} e^{:\phi_j:} e^{:f_{jk}:}. \tag{1}$$

By using the property of Lie transformations $e^{:-f:} e^{:g:} e^{:f:} = \exp\left(: e^{:-f:} g :\right)$, the e-cloud interaction can be "transported" to location k:

$$e^{:f_{ij}:} e^{:\phi_j:} e^{:f_{jk}:} = e^{:f_{ij}:} e^{:f_{jk}:} e^{-:f_{jk}:} e^{:\phi_j:} e^{:f_{jk}:} = \\ = e^{:f_{ij}:} e^{:f_{jk}:} \exp\left(: e^{:-f_{jk}:} \phi_j :\right). \tag{2}$$

The scalar potential ϕ_j is a function of transverse position coordinates x, y and of the longitudinal position with respect to the synchronous particle $\zeta = s - \beta_0 ct$, where s is the longitudinal position along the accelerator reference orbit, β_0 is the ratio between the particle's speed and the speed of light c, and t is time. According to the properties of Lie transformations:

$$e^{:-f_{jk}:} \phi_j(x, y, \zeta) = \phi_j(e^{:-f_{jk}:} x, e^{:-f_{jk}:} y, e^{:-f_{jk}:} \zeta). \tag{3}$$

In the Courant-Snyder parameterization of accelerator maps, the Lie transformation $e^{:f_{ij}:}$ can be written such that:

$$e^{:f_{ij}:} x = \sqrt{\frac{\beta_j}{\beta_i}} \left(\cos\mu_{ij} + \alpha_i \sin\mu_{ij}\right)(x - x_i) + \\ \sqrt{\beta_i \beta_j} \sin\mu_{ij} \left(p_x - p_{x,i}\right) + x_j, \tag{4}$$

where β_i and α_i are the betatron and alpha functions at locations i, respectively, μ_{ij} is the betatron phase advance between locations i and j, and $x_i, p_{x,i}$ are the coordinates of the closed orbit at locations i.

In addition, a typical characteristic of insertion regions with a small betatron function at the interaction point is that the phase advance remains practically unchanged until very close to the interaction point where it undergoes a rapid change of 180 degrees. This is certainly true for the LHC, and hence the phase advance inside the ITs is approximately zero. The longitudinal coordinate is to a good approximation unchanged within a single pass through the IT. This greatly simplifies Eq. (4), which becomes:

$$e^{:f_{ij}:} x = \sqrt{\frac{\beta_j}{\beta_i}} (x - x_i) + x_j. \tag{5}$$

Finally, the transformations related to the e-cloud $(e^{:\phi_i:})$ can all be transported to the same location. Because they are modelled as thin lenses, they commute and their scalar potentials can be added, to make an *effective* scalar potential Φ that describes the e-cloud interaction through all the slices of the IT:

$$\Phi(x, y, \zeta) = \\ \sum_i \phi_i \left(\sqrt{\frac{\beta_{x,i}}{\beta_{x,k}}} (x - x_k) + x_i, \sqrt{\frac{\beta_{y,i}}{\beta_{y,k}}} (y - y_k) + y_i, \zeta\right). \tag{6}$$

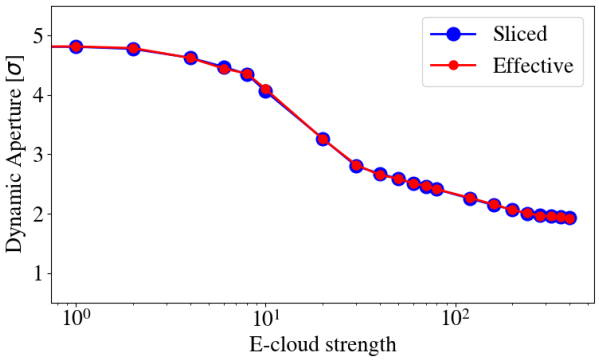

Figure 2: Dynamic aperture with respect to e-cloud strength using (blue) a sliced model and (red) an effective model.

Equation (6) can be used to evaluate the effective scalar potential in a three-dimensional grid and treat it as a typical scalar potential describing the e-cloud in one slice of the triplets.

As a benchmark, we compute the average dynamic aperture when including the e-cloud effect only in the "Q3" quadrupole of the IT on the right side of IP 1, with longitudinal position s between 46.965 m and 53.335 m (see Fig. 1). We choose this configuration because using special computers that have a capacity of up to 1 terabyte of random access memory, we are able to simulate the effect of the e-cloud in a "brute force" way without using Eq. (6). The dynamic aperture is then also computed by using only an effective e-cloud which has been computed using Eq. (6). The results are presented in Fig. 2, where the dynamic aperture is shown as a function of the "e-cloud strength" — a factor that is multiplied to scan the strength of the interaction. The blue points, which are computed from the "sliced" model, coincide with the red points, which are computed with the effective model of the interaction, validating the method of combining the different slices through Eq. (6).

BEAM DYNAMICS SIMULATIONS

In this section, we perform beam dynamics simulations including the effect of the beam-beam interaction, in order to compare the two effects. The e-cloud effect is represented by 4 effective e-clouds, each one corresponding to that of the IT left and right of IPs 1 and 5. The charge density distribution that corresponds to the scalar potential of the effective e-cloud in the IT right of 1, at $\zeta = 0$ is shown in Fig. 3. Typically in normal quadrupolar magnetic fields, the large electron densities are concentrated around the origin and around the diagonals [14]. Because of the aspect ratio

ISBN: 978-3-95450-247-9 ISSN: 2673-5490 doi: 10.18429/JACoW-IPAC2024-WEPR57

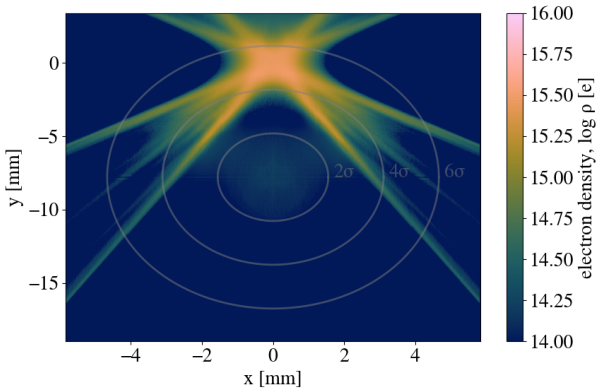

Figure 3: Snapshot (at $\zeta = 0$) of the electron density in the effective e-cloud in the IT right of IP 1.

between horizontal and vertical betatron functions, the large electron densities appear at different lines when represented by the effective model. It is clear that such an electron density will induce very non-linear forces, which are also time-dependent (dependent on ζ) [15].

The analysis of the beam dynamics is done through Frequency Map Analysis [16] (FMA) simulations and through computations of dynamic aperture while scanning the bunch intensity. Unless otherwise stated, the main parameters of the simulations consist of betatron tunes set to $(62.31, 60.32)$, chromaticity set to 20 units, lattice octupoles powered to 300 A, the half-crossing angle set to 160 µrad and betatron functions at the interaction points of 30 cm. The beam parameters are set to a bunch intensity of $1.2 \cdot 10^{11}$ p/b, transverse emittances of 2 µm, with r.m.s. bunch length equal to 0.09 m and a beam energy of 6.8 TeV. This configuration is typical of Run 3 when the luminosity levelling is finished [17]. The maximum secondary emission yield of the surface (relevant for the e-cloud buildup) is set to 1.3. Both head-on and long-range beam-beam interactions are included in the simulations.

The results of the FMA simulations are summarized in Fig. 4, where the effect of beam-beam interactions alone is shown in Fig. 4a, while the effect of e-cloud in the ITs is added in the simulations shown in Fig. 4b. It can be noted that the contribution of the e-cloud on the tune shift is small compared to that of beam-beam effects. Instead, the e-cloud appears to further excite resonances and increase the chaotic behaviour of high-amplitude particle orbits, visible through the stronger tune diffusion present in the FMA.

The average dynamic aperture as a function of the bunch intensity is plotted in Fig. 5. The e-cloud effect becomes smaller as the bunch intensity increases; an effect that is common for e-cloud buildup in quadrupole magnets at the LHC [18]. The e-cloud effect starts to overcome that of the beam-beam interaction at the lower end of bunch intensities (below $1.2 \cdot 10^{11}$ p/b), which is typically the intensity with which the LHC beams arrive at the end of the luminosity levelling [17]. It is important to note that the simulated configuration is not optimal for dynamic aperture. For this study, only the relative effect of the e-cloud is of interest.

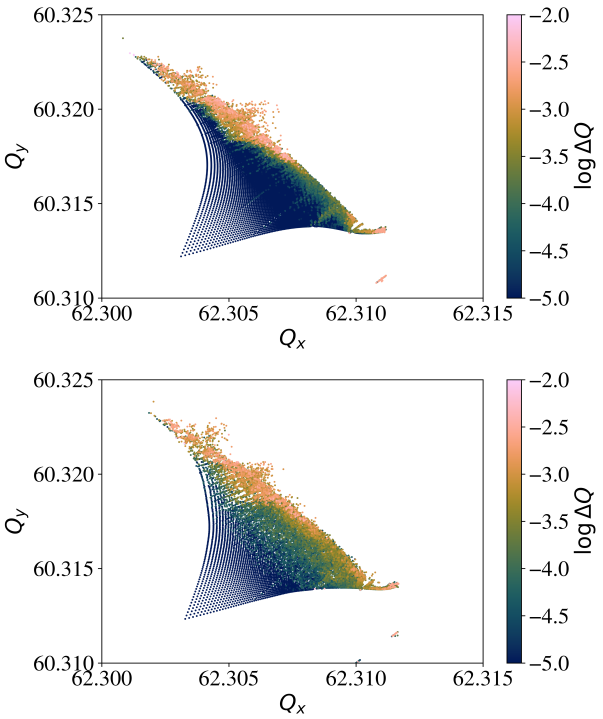

Figure 4: Frequency map analysis without (top) and with (bottom) e-cloud effects.

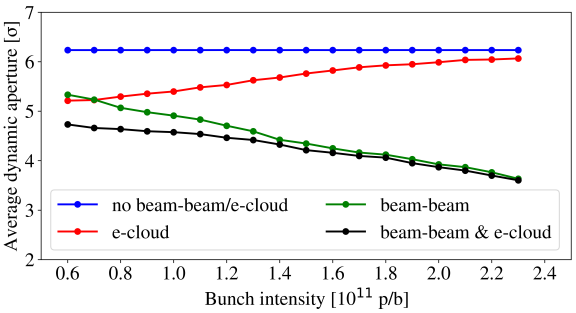

Figure 5: Dynamic aperture as a function of bunch intensity with and without beam-beam and e-cloud effects.

SUMMARY & OUTLOOK

This work enables the simulation of the incoherent effect of the e-cloud forming in the IT of the LHC by overcoming memory limitations. As was expected from measurements during Run 2 of the LHC, simulations show a significant impact on the dynamic aperture. Although only a small set of parameters were simulated, this work sets the basis for further exploration of incoherent e-cloud effects at the LHC.

The study of this type of e-cloud is particularly important for the HL-LHC [19] upgrade, as the upgrade relies on the complete suppression of the e-cloud formation through amorphous carbon coating of both new and existing IT beam chambers.

ACKNOWLEDGEMENTS

Research supported by the HL-LHC project. We thank Y. Papaphilippou, G. Rumolo, H. Bartosik, G. Franchetti, N. Mounet, R. Tomás, F. van der Veken and T. Persson for fruitful discussions.

ISBN: 978-3-95450-247-9 ISSN: 2673-5490 doi: 10.18429/JACoW-IPAC2024-WEPR57

REFERENCES

[1] K. Paraschou *et al.*, "Analysis on Bunch-by-Bunch Beam Losses at 6.5 TeV in the Large Hadron Collider", in *Proc. 10th Int. Particle Accelerator Conf. (IPAC'19)*, Melbourne, Australia, Jun. 2019, pp. 500–503. doi:10.18429/JACoW-IPAC2019-MOPMP029

[2] K. Paraschou and G. Iadarola, "Incoherent electron cloud effects in the Large Hadron Collider", in *Proc. of the ICFA mini-Workshop on Mitigation of Coherent Beam Instabilities in Particle Accelerators*, Zermatt, Switzerland, Sep. 2019, pp. 249–255. doi:10.23732/CYRCP-2020-009.249

[3] S. Kostoglou *et al.*, "Luminosity, lifetime and modelling", presented at the 9th LHC Operations Evian Workshop, Evian, France, Jan. 2019. https://indico.cern.ch/event/751857/contributions/3259405/.

[4] G. Iadarola *et al.*, "Progress in Mastering Electron Clouds at the Large Hadron Collider", in *Proc. IPAC'21*, Campinas, Brazil, May 2021, pp. 1273–1278. doi:10.18429/JACoW-IPAC2021-TUXA03

[5] G. Skripka and G. Iadarola, "Beam-induced heat loads on the beam screens of the inner triplets for the HL-LHC", CERN, Geneva, Switzerland, CERN-ACC-NOTE-2018-0009, 2018. https://cds.cern.ch/record/2305245

[6] K. Paraschou, "Studies of incoherent effects for the upgrade of the large hardon collider and detector applications", Ph.D. thesis, Aristotle University of Thessaloniki, Thessaloniki, Greece, 2023. doi:10.26262/heal.auth.ir.348933

[7] K. Paraschou and G. Iadarola, "A method for accurate and efficient simulations of slow beam degradation due to electron clouds", 2023. doi:10.48550/arXiv.2302.10581

[8] K. Paraschou *et al.* "Emittance Growth From Electron Clouds Forming in the LHC Arc Quadrupoles,", in *Proc. HB'23*, 2024, pp. 487–490. doi:10.18429/JACoW-HB2023-THBP16

[9] G. Iadarola *et al.*, "Xsuite: an integrated beam physics simulation framework", presented at HB'23, Geneva, Switzerland, Oct. 2023, paper TUA2I1.

[10] G. Iadarola *et al.*, "Evolution of Python Tools for the Simulation of Electron Cloud Effects", in *Proc. IPAC'17*, Copenhagen, Denmark, May 2017, pp. 3803–3806. doi:10.18429/JACoW-IPAC2017-THPAB043

[11] W. Herr, "Mathematical and Numerical Methods for Nonlinear Beam Dynamics", in *Proc. 2018 course on Numerical Methods for Analysis, Design and Modelling of Particle Accelerators*, Thessaloniki, Greece, Nov. 2018. https://cds.cern.ch/record/2723693

[12] Y. Papaphilippoum and F. Zimmermann, "Weak-strong beam-beam simulations for the Large Hadron Collider", *Phys. Rev. Spec. Top. Accel. Beams*, vol. 2, p. 104001, 1999. doi:10.1103/PhysRevSTAB.2.104001

[13] G. Iadarola, "Modelling the interaction of a relativistic beam particle with an electron cloud", CERN, Geneva, Switzerland, CERN-ACC-NOTE-2019-0033, 2019. https://cds.cern.ch/record/2684858

[14] R. J. Macek *et al.*, "Electron cloud generation and trapping in a quadrupole magnet at the Los Alamos proton storage ring", *Phys. Rev. Spec. Top. Accel. Beams*, vol. 11, p. 010101, 2008.

[15] E. Benedetto and F. Zimmermann, "Analysis of the electron pinch during a bunch passage", in *Proc. 31st Advanced ICFA Beam Dynamics Workshop on Electron-Cloud Effects (ECLOUD'04)*, Napa, USA, Apr. 2004, 2005, pp. 81–87. doi:10.5170/CERN-2005-001.81

[16] Y. Papaphilippou, "Detecting chaos in particle accelerators through the frequency map analysis method", *Chaos*, vol. 24, p. 024412, 2014. doi:10.1063/1.4884495

[17] S. Fartoukh *et al.*, "LHC Configuration and Operational Scenario for Run 3", CERN-ACC-2021-0007, Geneva, 2021. https://cds.cern.ch/record/2790409

[18] G. Skripka *et al.*, "Non-monotonic dependence of heat loads induced by electron cloud on bunch population at the LHC", *Eur. Phys. J. Plus* vol. 137, p. 849, 2022. doi:10.1140/epjp/s13360-022-02929-8

[19] O. Aberle *et al.*, "High-Luminosity Large Hadron Collider (HL-LHC): Technical Design Report", CERN, Geneva, Switzerland, CERN-2020-010, 2020. doi:10.23731/CYRM-2020-0010